European Journal of Pharmacology 1014 (2026) 178524

Contents lists available at ScienceDirect

European Journal of Pharmacology

journal homepage: www.elsevier.com/locate/ejphar

# The new *vrdg*183 toxin from the Colombian spider *Pamphobeteus verdolaga* inhibits L-type $Ca^{2+}$ currents through an allosteric mechanism

Alejandro Gómez-Restrepo [a,1], Jessica Rojas-Palomino [b,1], Cristian Salinas-Restrepo [c], César Segura [d], Oscar A. Saurith-Coronell [e,f], Edgar A. Márquez-Brazón [e], Marco A. Giraldo [b], Juan C. Calderón [a,*]

[a] Physiology and Biochemistry Research Group−PHYSIS, Faculty of Medicine, University of Antioquia, Medellín, 050010, Colombia
[b] Group of Biophysics, Institute of Physics, University of Antioquia, Medellín, 050010, Colombia
[c] Toxinology, Therapeutic and Food Alternatives Research Group, Faculty of Pharmaceutical and Food Sciences, University of Antioquia, Medellín, 050010, Colombia
[d] Malaria Group, Faculty of Medicine, University of Antioquia, Medellín, 050010, Colombia
[e] Grupo de Investigación en Química y Biología, Departamento de Química y Biología, Universidad del Norte, Barranquilla, 081007, Colombia
[f] Departamento de Medicina, Facultad de Ciencias de la Salud, Universidad del Norte, Barranquilla, 081007, Colombia

A R T I C L E I N F O

*Keywords:*
Spider toxin
$Ca^{2+}$ channel
$K^{+}$ channel
Patch-clamp
Docking
Molecular dynamics
Calciseptine

A B S T R A C T

*Background:* Spider venoms are enriched in toxins that modulate mammalian voltage-gated ion channels (VGIC) with pharmacological potential. However, the inventory of toxins of American spiders with effects on voltage-gated $Ca^{2+}$ channels has lagged the number of toxins interacting with other channels. Here, we aimed at identifying new $Ca^{2+}$ channel-modulating toxins of the Colombian spider *Pamphobeteus verdolaga*.
*Methods:* The sequences of five novel short, positively charged, disulfide-bridged peptides, and one more short, non-bridged control peptide, were selected from the transcriptomic database of the venom gland of *P. verdolaga*. Peptides were synthesized and screened at 1 μM for their effects on L-type $Ca^{2+}$ currents ($I_{CaL}$) in mouse cardiomyocytes using patch-clamp. $I_K$ were also evaluated to gain information about the selectivity of the peptides. 3D modeling, docking and molecular dynamics simulations were likewise performed.
*Results:* *vrdg*183 (19 amino acid residues, four cysteines, charge +7, 2.33 kDa), followed by *vrdg*69 and *vrdg*177, inhibited over 60 % of $I_{CaL}$. *vrdg*172 and *vrdg*164 showed a moderate effect of less than 40 %. *vrdg*183 had a half-maximal inhibitory concentration for $I_{CaL}$ of 858.28 nM and was the only toxin lacking effect on $I_K$. *vrdg*183, consisting of two antiparallel β-strands, was successfully docked to the extracellular $L6_{IV}$ loop at the outer pore region of the human cardiac $Ca_v1.2$ with a binding energy of −9.5 kJ/mol. **Conclusion**: This is the first report of toxins of *P. verdolaga* with effects on VGIC. *vrdg*183 highlights as a very low molecular weight, moderately potent $I_{CaL}$ inhibitor through an allosteric mechanism, without effect on $I_K$.

## 1. Introduction

Many animal venoms are enriched in mammalian voltage-gated ion channel (VGIC)-modulating peptide toxins (Bolon et al., 2023; Langenegger et al., 2019; Rash and Hodgson, 2002; Rojas-Palomino et al., 2024). In invertebrates, including the Arthropoda phyla, these toxins are typically made of 10–75 amino acids and give origin to a large and complex structural diversity (Daly and Craik, 2011; Jin et al., 2019; King and Hardy, 2013; Langenegger et al., 2019; Quintero-Hernández et al., 2013; Xia et al., 2023). Ultimately, their low molecular weight (MW) (<10 kDa), the presence of disulfide bridges and the folding patterns favored by them confer many toxins with stability and affinity to bind and modulate VGIC (Deplazes, 2017; Langenegger et al., 2019; Quintero-Hernández et al., 2013; Rojas-Palomino et al., 2024).

Mammalian VGIC are multispanning, multisubunit membrane proteins specialized in allowing the passage of ions across the cell membrane in favor of an electrochemical gradient. Although VGIC are enriched in excitable cells, they can also be present in many other cell types (Bolaños and Calderón, 2022; Catterall, 1995; Quintana et al., 2010). VGIC are composed of either a large, monomeric α-subunit or a

* Corresponding author.
*E-mail address:* jcalderonv00@yahoo.com (J.C. Calderón).
[1] These authors contributed equally to this work.

https://doi.org/10.1016/j.ejphar.2026.178524
Received 10 October 2025; Received in revised form 10 December 2025; Accepted 6 January 2026
Available online 7 January 2026

polymeric α-subunit made of smaller subunits. Voltage-gated $Ca^{2+}$ channels (VGCC) represent the first structure and voltage-gated $K^{+}$ channels (VGKC) are the prototype of the second. The α-subunit is particularly important for the movement of ions across the membrane because it harbors the pore domain (PD) and the positively charged S4 helices of the voltage sensing domain (VSD) (Bezanilla, 2008; Rojas-Palomino et al., 2024; Wu et al., 2016). Accessory subunits also influence the biophysical properties of the channels (Morin and Kobertz, 2008).

Many Central and South American cnidarians, cone snails, snakes, scorpions and spider toxins have been reported to modulate mammalian VGIC: in up to 95 % of the cases the result is a reduction of the current flowing through the channel (Rojas-Palomino et al., 2024). Moreover, ~65 % of the toxins characterized in these geographical regions come from scorpions and only ~15 % come from spiders. Of those toxins, 90 % have been either tested only against VGKC or found to modulate only VGKC (Rojas-Palomino et al., 2024).

Recently, our transcriptomic analyses of the venom gland of *Pamphobeteus verdolaga,* a spider species discovered in Colombia (Cifuentes et al., 2016), revealed novel short polypeptide sequences with cysteine residues putatively involved in disulfide bridges, showing identity with other spider toxins (Salinas-Restrepo et al., 2022, 2024). Moreover, preliminary fluorescence assays suggested that some fractions of the venom of this spider could block VGCC (Estrada-Gomez et al., 2019), with the specific VGIC-interacting toxins yet to be identified. This led us to hypothesize that the venom gland of *P. verdolaga* has toxins with direct effect on mammalian VGCC with potential pharmacological applications. Here, we report the synthesis, purification and electrophysiological evaluation of five bridged and one non-bridged novel toxins of the venom gland of *P. verdolaga,* demonstrating their effects as VGIC regulators. Furthermore, the most selective toxin was *in silico* characterized to unveil its mechanism of action on the human VGCC cardiac isoform.

## 2. Materials and methods

### Ethical approval

All experimental procedures involving animals in this research were approved by the institutional Committee for Ethics in Experiments with animals of the University of Antioquia (minutes 129 of October 29th of 2019), Colombia, according to the Law 84 of 1989 and Resolution 8430 of 1993, and were performed in compliance with the Directive 2010/63/EU of the European Parliament guidelines, as well as policies on experimental design and analysis and reporting of the results (Percie du Sert et al., 2020). Animals were kept in polypropylene cages with ad libitum access to food and water under 12:12 h light:dark cycles. Only adult, male Swiss Webster mice, weighing 20–26 g, were used. For euthanasia, animals were exposed to 2 % isoflurane for 25–30 s followed by a rapid cervical dislocation performed by a trained researcher.

### 2.1. Peptides synthesis

The previous use of three distinct assembly algorithms and the merging of each of their non-redundant outputs allowed our group to identify more than 18.000 sequences and 260 putative new toxins in the venom gland of the spider *P. verdolaga* (Salinas-Restrepo et al., 2022). Six of those new peptides were chosen for this study based on their predicted physicochemical properties (*vrdg*66, *vrdg*69, *vrdg*164, *vrdg*172, *vrdg*177 and *vrdg*183) and were synthesized as we recently reported (Salinas-Restrepo et al., 2024). Briefly, solid-phase peptide synthesis (SPPS) methods following a standard Fmoc/tBu protocol using Rink MBHA resin (Millipore, Germany) as solid support (Guzmán et al., 2021) were used. Deprotection was carried out under agitation at room temperature (RT) in two 20-min cycles of 10 % w/v piperazine in 10 % v/v ethanol in N,N-dimethylformamide. The Fmoc-L-amino acids, activators and coupling agents (N-[(1H-benzotriazol-1-yl)-(dimethylamino)methylene]-N-methylmethanaminium hexafluorophosphate N-oxide —HBTU—, Oxyma Pure® and N,N-diisopropylethylamine —DIPEA—, Millipore) were used in a 10-fold excess. Five-hour coupling cycles were employed under agitation and RT for HBTU. Coupling completion was monitored by the absence of bromophenol blue coloration. After the required elongation, the peptides were cleaved from the solid support for 2 h under agitation at RT using a 92.5:2.5:2.5:2.5 solution of trifluoroacetic acid (TFA)/triisopropylsilane (TIS)/2-mercaptoethanol/$H_2O$, respectively. Peptides were precipitated and removed from the cleavage solution, dissolved in ultra-pure water, frozen at −70 °C and lyophilized for storage.

The purity and identity of the peptides was verified by using reverse-phase high performance liquid chromatography (RP-HPLC) and mass spectrometry (MS), as described (Salinas-Restrepo et al., 2024). Briefly, a 1 μg/μL stock of the peptides was prepared in a 0.05 % v/v TFA water solution, and analyzed on a JASCO Corp HPLC (JASCO Corp, Tokyo, Japan) with an XBridgeTM BEH C18 column (Waters Corporation, Milford, Massachusetts, USA). Peptide monitoring was conducted at 214 nm. Identity verification was carried out using MS on a LC/MS-2020 ESI-MS device (Shimadzu Corp., Kyoto, Japan). The run consisted of a 0–70 % 0.05 % v/v TFA acetonitrile gradient at 1 mL/min for 20 min at 4.5 kV and 350 °C.

The formation of disulfide bridges was carried out according to the protocol published by Zhang et al. (2010). Peptides were dissolved in a 5 mM guanidine-HCl, 10 % v/v DMSO aqueous solution to a concentration of 0.20 mg/mL, pH 7.0. Oxidation was accomplished at 300 rpm (SH-200, Cole-Parmer Instrument Company, Vernon Hills, IL, USA) for 16 h at RT. Following lyophilization, the peptides were purified and guanidine and DMSO were removed by solid phase extraction with RP-18 cartridges (Merck, Germany) using acetonitrile with 10 % increments until 100 % v/v. Purity was expected to be over 90 % for all peptides and no further analyses were systematically performed to verify the formation of disulfide bridges or to detect changes in mass due to possible oligomerization.

### 2.2. Cardiomyocyte's isolation

Following the method described by our laboratory (Rojas-Palomino et al., 2024), hearts were rapidly dissected out from the mice and immersed twice in filtered, cold, $Ca^{2+}$-free Tyrode's solution (in mM: NaCl 135, KCl 5.4, $MgCl_2$ 1, glucose 10, HEPES 10, $NaH_2PO_4$ 0.33, pH 7.2) supplemented with enoxaparin (1 mg/mL). The aorta was then cannulated under magnification, mounted on a Langendorff apparatus and perfused at a constant flow rate of 4.5 mL/min with $Ca^{2+}$-free Tyrode's solution bubbled with 95 % $O_2$ and 5 % $CO_2$. This solution was supplemented with 1 mg/mL collagenase type 2 (Worthington, Lakewood, NJ, USA) and 0.1 mg/mL protease type XIV (Sigma, St. Louis, MO, USA), at 37 °C for ~19–20 min. The ventricles were then gently triturated and agitated with fine forceps to obtain isolated single cardiomyocytes. $Ca^{2+}$ was then slowly restored to the solution. Only freshly isolated, striated, brick-shaped cardiomyocytes, with intact bright membrane and without spontaneous contractions were selected for the experiments.

### 2.3. Electrophysiology assays

The fact that preliminary evidence suggests the presence of toxins blocking VGCC in venom fractions of *P. verdolaga* (Estrada-Gomez et al., 2013, 2019), and most toxins discovered in America have been reported to target $I_K$ (Rojas-Palomino et al., 2024), prompted us to specifically look for toxins targeting $I_{Ca}$. Complementary $I_K$ analyses were performed to conclude on the specificity of the effects.

Macroscopic $Ca^{2+}$ ($I_{Ca}$) and $K^{+}$ ($I_K$) currents were recorded in the isolated cardiomyocytes using the whole-cell configuration in voltage-clamp mode of the patch-clamp technique (Multiclamp 700B, Axon

Instruments, USA) (Conforti, 2012; Hamill et al., 1981; Kodirov, 2023; Rojas-Palomino et al., 2024). Microelectrodes with open-tip bath resistances of 2–2.5 MΩ were obtained from Schott 8250 glass capillaries (593800, A-M Systems, USA) using a horizontal puller (PUL-1000, WPI, USA) and a microforge (MF 200-1, WPI).

For $I_{Ca}$ recordings, the pipette solution contained (mM): HEPES 11, EGTA 10, CsCl 125, MgATP 5 (pH 7.1, adjusted with CsOH) and the bath solution had (mM): tetraethylammonium (TEA) chloride 140, $MgCl_2$ 1, CsCl 6, $CaCl_2$ 1, HEPES 10, glucose 10 (pH 7.4 with CsOH) (Lacampagne et al., 1995). $I_{Ca}$ were elicited with 100 ms voltage steps from −40 to +60 mV in 10 mV increments from a holding potential of −50 mV. Nifedipine (5 and 13 μM) or isoproterenol (10–100 μM) were used in control experiments to confirm the identity of the current.

To evaluate $I_K$, the pipette solution contained (mM): KCl 140, $MgCl_2$ 2, MgATP 4, EGTA 5, HEPES 10 (pH 7.2 with KOH) and the bath solution had (mM): NaCl 135, KCl 5.4, $MgCl_2$ 1, glucose 10, HEPES 10, $NaH_2PO_4$ 0.33, tetrodotoxin 0.1 (pH 7.2 with NaOH). Nifedipine 10 μM was added to the bath solution only if needed. $I_K$ were activated with a protocol of 100 ms voltage steps from −30 mV to +80 mV in 10 mV increments from a holding potential of −40 mV. TEA (150 mM) or phrixotoxin 2 (PaTx2, 200 nM) (Diochot et al., 1999) were used to confirm the identity of the current.

Currents were recorded and stored using the Clampex v10.5 software (Molecular Devices, USA), at 10 kHz and low-pass filtered at 5 kHz. The series resistance of the pipettes was compensated at a maximum of 50 % and the P/4 protocol was used to subtract leakage currents. Only recordings obtained with a membrane seal resistance (Rt) over 1 GΩ, an access resistance (Ra) lower than 10 MΩ, a membrane capacitance (Cm) over 100 pF and deemed negligible leak current were included in the analyses, ensuring only results with good voltage control. Current densities (pA/pF) (Kodirov, 2023) were used for non-paired analysis (controls, pharmacological characterizations, concentration-response curve) to account for cell-to-cell variability. For paired analysis (screening of the peptides), data was normalized to the peak current amplitude of the controls. All experiments were conducted at RT (22–24 °C).

The lyophilized peptides were reconstituted in deionized water, divided into aliquots and stored at −80 °C. On the day of the experiment, individual aliquots of peptides were slowly thawed on ice and carefully added to the bath solution at a final concentration of 1 μM for screening. In further concentration-response experiments, the cardiomyocytes were exposed to increasing concentrations of *vrdg*183 in independent assays.

### 2.4. In silico three-dimensional structures and molecular docking

The amino acid sequences of *vrdg*183, published by our group (Salinas-Restrepo et al., 2024), and calciseptine (UniProt P22947), a snake toxin used as a positive control known to specifically block $Ca_v1.2$ (de Weille et al., 1991; Gao et al., 2023; Mesirca et al., 2024), served as input for pyPept (Ochoa et al., 2023) and AlphaFold 3 (Abramson et al., 2024) softwares to generate their three-dimensional (3D) structures. The 3D models with the highest prediction scores were selected and saved as .pdb format. The 3D structure of the human cardiac $Ca_v1.2$ isoform (UniProt Q13936) was retrieved from the Protein Data Bank (PDB ID 8WE6, https://www.rcsb.org/, accessed May 2025). Crystallographic water molecules, non-protein components and subunits not expected to be directly involved in the toxin-channel interaction were removed using AutoDock tools. Finally, only the α1C subunit, recognized as the primary binding interface for multiple inhibitors (Gao et al., 2023), was retained.

To evaluate the most accurate toxins-channel docking protocol, we employed the two widely used platforms ClusPro 3.0 (Porter et al., 2017) and HDOCK (Yan et al., 2020). Each platform's docking results underwent comparison to the experimentally resolved reference structure of the calciseptine-$Ca_v1.2$ complex (PDB ID 8WE7) while focusing on spatial orientation and peptide binding interface. Thus, for the *vrdg*183-$Ca_v1.2$ docking we chose the method that produced the calciseptine-$Ca_v1.2$ pose closest to the experimentally determined complex.

### 2.5. Molecular dynamics

The molecular dynamics (MD) simulations aimed to evaluate the structural stability and binding behavior of the toxin-channel complexes under conditions that mimic the mammalian physiological environment. All protocols were executed using the YASARA Structure software, employing the AMBER14 force field, following previously established methodologies (Sierra-Hernandez et al., 2025). Once docked, each toxin-channel complex was placed in a cubic simulation box, leaving a 5 Å buffer around the molecules to ensure proper solvation. We applied periodic boundary conditions to simulate a continuous environment and reduce edge effects. The systems were solvated with explicit water molecules, and $Na^+$ and $Cl^-$ ions were added to reach a physiological extracellular concentration of 0.9 %. All simulations were run at 298.15 K and the pressure was adjusted at 1 atm based on the density of water (0.997 g/ml).

Before the production run, each system underwent energy minimization and equilibration. The production phase lasted 100 ns for each complex, using a 1.25 fs time step.

After the simulations, we analyzed the trajectories using YASARA's built-in macros. We focused on root mean square deviation (RMSD) and Radius of gyration (Rg) to assess structural stability and flexibility. To estimate binding strength, the energy terms values were extracted from the trajectories using the md_analyzebindenergy.mcr macro, which incorporates the Poisson-Boltzmann Solver (APBS) for electrostatic calculations, based on the Molecular Mechanics Poisson-Boltzmann Surface Area (MM-PBSA) method.

The binding energy was calculated as:

$$\text{Binding energy} = \Delta\text{Esolvation} + \Delta\text{Epotential} \quad (1)$$

$$\text{Where: } \Delta\text{Esolvation} = \text{Esolv, complex} - (\text{Esolv, channel} + \text{Esolv, toxin}) \quad (2)$$

$$\Delta\text{Epotential} = \text{Epot, complex} - (\text{Epot, channel} + \text{Epot, toxin}) \quad (3)$$

This formulation captures the energetic contributions from both solvation (Esolv) and molecular interactions (Epot) during complex formation.

### 2.6. Data analysis and statistics

Recordings were analyzed with Clampfit v10.5 (Molecular Devices, USA) and graphed with Origin Pro2019 (Origin Lab Corporation, Northampton, MA, USA) or GraphPad Prism v10.0 (GraphPad, Boston, MA, USA). Results of the screening include three to six independent, paired experiments. The activation phase of the currents (*i.e.*, from the starting point of the recording to the point of maximum amplitude) was described by the $\tau_{act}$ values of a decay fitted exponential function. In the concentration-response experiments, data was fitted with the sigmoidal function:

$$y = A1 + \frac{A2 - A1}{1 + 10^{(Log\ x_0 - x)p}} \quad (4)$$

The value of $Logx_0$ was considered the inhibitory concentration 50 ($IC_{50}$) and *p* represents the Hill slope. All results are expressed as means ± standard error of the mean (SEM). Statistical differences were assessed using paired or non-paired t-tests for two-group comparisons and one-way ANOVA followed by Tukey's post hoc test for analyses involving more than two groups. Normality was verified with the Shapiro-Wilk test. Differences were considered significant at $P < 0.05$.

**Table 1**
Physicochemical properties of the *P. verdolaga* novel peptides evaluated in this study[a].

| Peptides | Amino acids sequence | Disulfide bridges | MW (kDa) | Hydrophobic moment | Charge | Isoelectric point | Solubility (mg/ml) |
|---|---|---|---|---|---|---|---|
| ***vrdg*66** | WKKIKKFF | 0 | 1.12 | 0.37 | +5 | 11.2 | >8 |
| ***vrdg*69** | YRARCVIYC | 1 | 1.15 | 0.06 | +3 | 8.7 | 2 |
| ***vrdg*164** | RSVLKAHCRICRRRG | 1 | 1.81 | 0.07 | +7 | 10.8 | 2 |
| ***vrdg*172** | CRKLCFRNRCLTYCRGR | 2 | 2.15 | 0.06 | +7 | 9.8 | 4 |
| ***vrdg*177** | QCRKLCFRNRCLTYCRGR | 2 | 2.28 | 0.06 | +7 | 9.8 | 4 |
| ***vrdg*183** | QCRKLCFRNRCLTYCRGRG | 2 | 2.33 | 0.06 | +7 | 9.8 | 4 |

[a] *vrdg* states for *verdolaga*. MW: theoretical molecular weight.

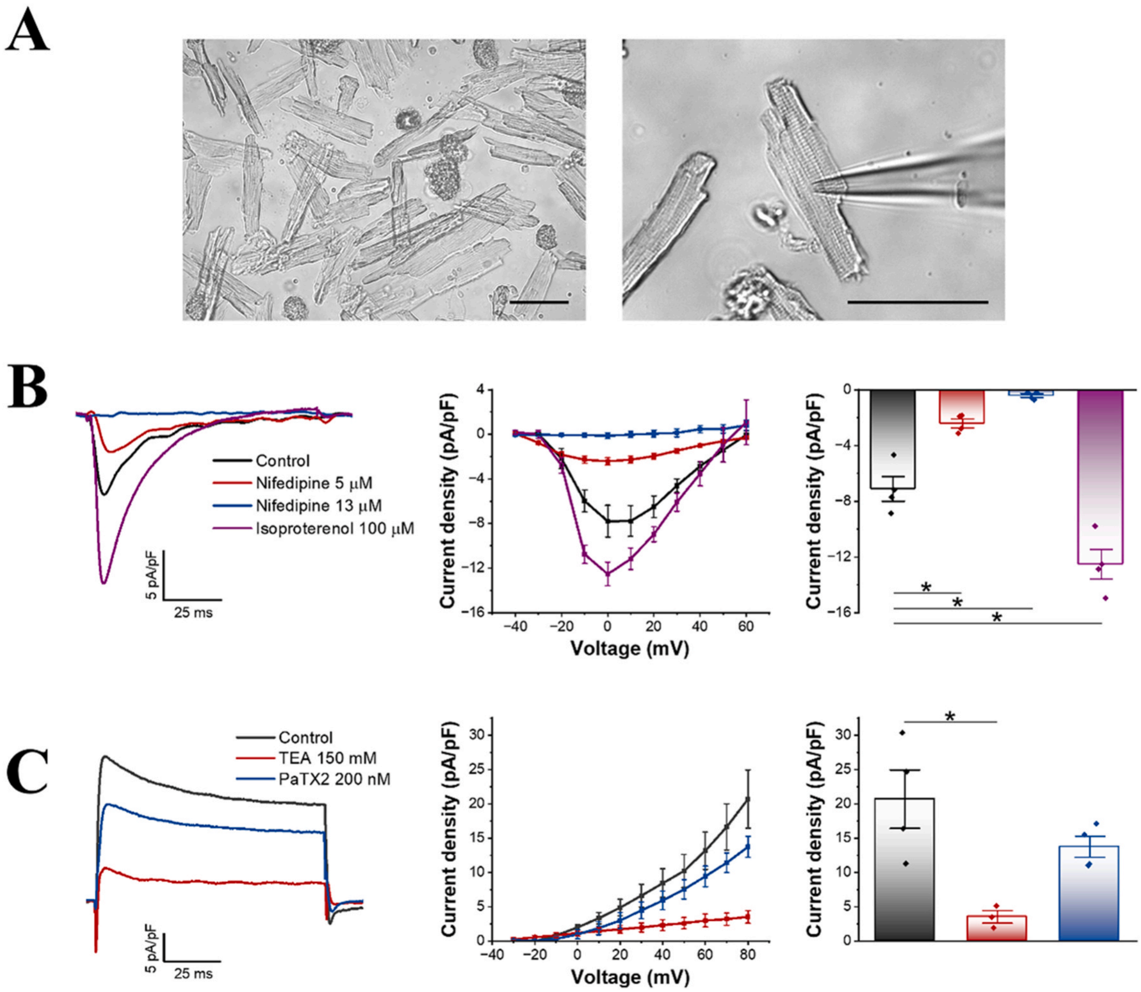


**Fig. 1.** Characterization of $I_{Ca}$ and $I_K$ obtained in ventricular cardiomyocytes of mice using patch-clamp. A. The panel on the left illustrates the typical appearance of recently isolated ventricular cardiomyocytes under low magnification. On the right a representative patched cardiomyocyte is shown. The cell is in the middle and the micropipette comes from the right. Scale bars: 100 µm. **B.** The leftmost panel shows representative recordings of the effect of nifedipine or isoproterenol on $I_{Ca}$ at 0 mV. Although the traces for nifedipine and isoproterenol were obtained in independent experiments, they were ensembled for an easier comparison. The panel in the middle depicts the current to voltage (I–V) plots for n = 4 different cells per condition. The rightmost panel shows the grouped results. Nifedipine reduced the mean peak $I_{Ca}$ current density in a concentration-dependent manner: from −7.1 ± 0.88 pA/pF under control conditions to −2.41 ± 0.32 pA/pF at 5 µM and to −0.41 ± 0.13 pA/pF at 13 µM. Conversely, 100 µM isoproterenol markedly enhanced the current to −12.52 ± 1.06 pA/pF (*P < 0.05, one-way ANOVA followed by Tukey's post-hoc test). The results confirm the identity of the current as $I_{CaL}$. **C.** The panel on the left illustrate representative results of the effect of the pharmacological modulators tetraethylammonium (TEA) and Phrixotoxin 2 (PaTX2) on $I_K$ at +80 mV evaluated in independent experiments. Mean I-V plots for n = 3–4 different cells per condition are shown in the middle. The grouped results on the right show that TEA decreased the current density to 3.5 ± 0.92 pA/pF compared to a control $I_K$ of 20.67 ± 4.25 pA/pF. PaTX2 decreased the current to 13.71 ± 1.53 pA/pF (*P < 0.05, one-way ANOVA followed by Tukey's post-hoc test). These results confirm that $I_K$ comes from different $K_v$ isoforms, including $K_v$4.x.

## 3. Results

### 3.1. Peptides

Table 1 summarizes the physicochemical properties of the different peptides chosen for this study. *vrdg*66 served as a control because it matches key properties with the other peptides, such as a positive charge, good solubility and a very low MW, but was not expected to affect VGIC because it lacks disulfide bridges. In contrast, the remaining five bridged-peptides were expected to modulate VGIC in

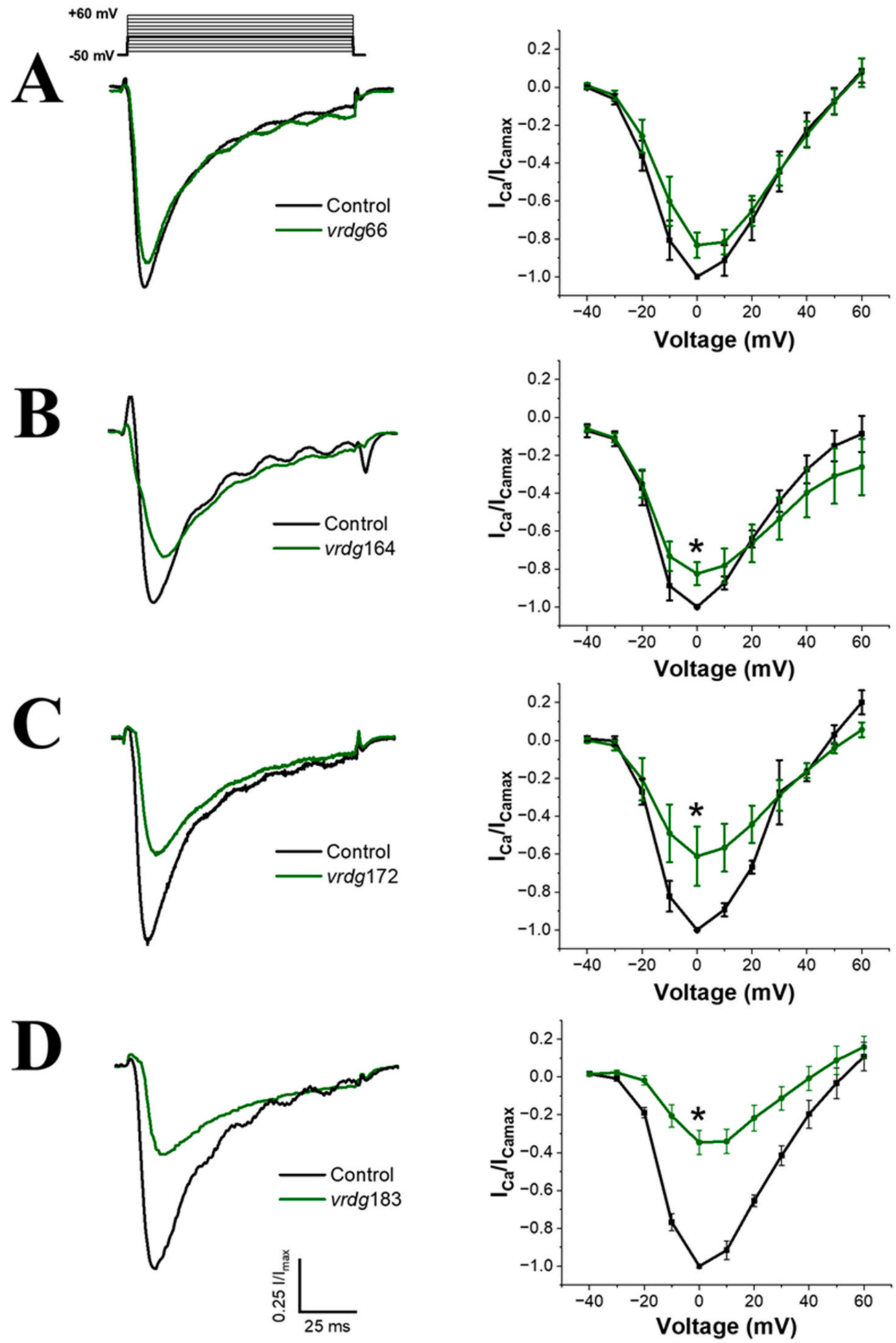


**Fig. 2. Selected normalized mean traces showing the effect of the *P. verdolaga* peptides on $I_{CaL}$.** Mean traces were generated by pooling all control (black) or experimental (*vrdg* peptides, green⁋) records in one trace (left column), to summarize the effect of *vrdg*66 (**A**), *vrdg*164 (**B**), *vrdg*172 (**C**) and *vrdg*183 (**D**) on $I_{CaL}$ at 0 mV. The scale bar applies to all panels in the left column. The right column shows the corresponding current to voltage plots of the same toxins illustrated on the left. *vrdg*69 and *vrdg*177 were not shown because they look like the records of *vrdg*183. The upper insert represents the voltage step protocol used for stimulation. ⁋All traces from the spider toxins are identified in green in this and subsequent figures because the Spanish word "verdolaga" means greenish. *P < 0.05, paired Student's *t*-test for current at 0 mV. $I_{CaL}$: L-type $Ca^{2+}$ current. (For interpretation of the references to color in this figure legend, the reader is referred to the Web version of this article.)

cardiomyocytes.

### 3.2. Cardiomyocytes and control currents

Representative images of the cardiomyocytes used for the experiments are shown in Fig. 1A. Three lines of evidence confirm that these cardiomyocytes gave macroscopic L-type $I_{Ca}$ ($I_{CaL}$) mostly carried by the $Ca_v1.2$ isoform (Alexander et al., 2021; Grunnet, 2010; Hussain and Orchard, 1997): i) their inward current peaked between 0 and +10 mV, as shown in the current to voltage (I-V) plot, ii) were completely inhibited by nifedipine, and iii) were activated by isoproterenol (Fig. 1B).

Many $I_K$ are activated in these cardiomyocytes under the protocols used in this study (Grunnet, 2010; Rojas-Palomino et al., 2024). Given

**Table 2**
Summary of the effects of the *P. verdolaga* peptides on $I_{CaL}$ and $I_K$ in mice cardiomyocytes.[a]

| Peptides | $I_{CaL}$ | | | $I_K$ | | |
|---|---|---|---|---|---|---|
| | n | Inhibition (%) | SEM (%) | n | Inhibition (%) | SEM (%) |
| *vrdg*66 | 6 | −16.3 | 10.5 | 5 | −24.4 | 4.4 |
| *vrdg*69 | 4 | −63.3 | 12.7 | 4 | −52.5 | 6.3 |
| *vrdg*164 | 5 | −17.4 | 6.1 | 3 | −14.4 | 12.7 |
| *vrdg*172 | 4 | −38.8 | 15.6 | 3 | −43.9 | 5.8 |
| *vrdg*177 | 3 | −61.8 | 10.9 | 3 | −40.9 | 10.1 |
| *vrdg*183 | 4 | −66.7 | 6.5 | 3 | −6.2 | 24.6 |

[a] *vrdg* states for *verdolaga*. n refers to the number of independent experiments. Values in columns 3 and 6 are negative to express the percentage of inhibition of the indicated current. $I_{CaL}$: L-type $Ca^{2+}$ current. $I_K$: $K^+$ current. SEM: standard error of the mean.

the kinetics, the partial response to high concentrations of TEA and its sensitivity to PaTx2, this current is likely carried out by $K_v4.2$ ($I_{to,f}$), $K_v4.3$ ($I_{to,f}$), $K_v1.4$ ($I_{to,s}$), $K_v1.5$ and $K_v1.7$ (Fig. 1C). Thus, we will continue generalizing this current as $I_K$.

### 3.3. Differential effect of the vrdg peptides on $I_{CaL}$ in mice cardiomyocytes

The screening at 1 μM identified *vrdg*183 as the most effective peptide inhibitor of $I_{CaL}$, followed by *vrdg*69 and *vrdg*177, all over 60 %. In contrast, *vrdg*172 and *vrdg*164 produced a moderate inhibition of less than 40 % (Fig. 2 and Table 2). As expected, *vrdg*66 had no significant effect on $I_{CaL}$. Only *vrdg*164 lengthened the activation phase of the current ($\tau = 4.45 \pm 0.72$ vs $\tau = 2.64 \pm 0.49$ ms in the control, $P = 0.03$) (Fig. 2). All effects appeared within 5 min of incubation with the toxins.

### 3.4. Differential effect of the vrdg peptides on $I_K$ in mice cardiomyocytes

*vrdg*69, *vrdg*172 and *vrdg*177 at 1 μM inhibited over 40 % $I_K$. The remaining peptides inhibited less than 25 % of the current (Fig. 3 and Table 2). Notably, *vrdg*183 had no effect on $I_K$. Similarly, the effects appeared within 5 min of exposure to the toxins.

### 3.5. The new spider toxin vrdg183 has moderate potency to inhibit $I_{CaL}$ in mice cardiomyocytes

Given its pronounced and selective effect on $I_{CaL}$, *vrdg*183 was considered the most promising toxin for further characterization. First, we corroborated the inhibitory effect of *vrdg*183 on $I_{CaL}$ in cardiomyocytes previously exposed to isoproterenol using a design of repeated measurements. The results shown in Fig. 4A fully confirm the effect of *vrdg*183 and the good health of the cardiomyocytes employed in the assays.

An $IC_{50}$ of 828.28 nM was then estimated by fitting the concentration-response data. These results also indicate that this peptide does not affect the activation voltage at any tested concentration (Fig. 4B–D).

### 3.6. 3D structures and molecular docking

The model generated by AlphaFold 3 exhibited the lowest RMSD (3.8 Å compared to 8.7 Å for the pyPet structure) relative to the experimental calciseptine structure, indicating the highest structural fidelity (Fig. 5A). Based on this, AlphaFold 3 was selected as the preferred tool for modeling the 3D structure of *vrdg*183. As expected from its length and the presence of four cysteine residues, *vrdg*183 assembles into a structure of two antiparallel β-strands linked by a short loop and stabilized by two disulfide bridges (Cys2-Cys15 and Cys6-Cys11). The C-terminal region conformed in a longer and freer loop than the N-terminal (Fig. 5B). Intramolecular hydrogen bonds also stabilize the structure (Table 3). The molecular surface area was 2016.02 $Å^2$.

The satisfactory structures of the toxins were thus docked into the $Ca_v1.2$ channel and the results were ranked according to their scores. Table 4 reveals the top scoring values in each case, confirming the high quality of the models. The confidence scores obtained with HDOCK were slightly larger than those obtained with ClusPro, thus HDOCK models were expected to be more reliable. Moreover, HDOCK was able to predict the experimentally identified channel binding site of calciseptine (Fig. 5C and E). Thus, a further structural evaluation of the HDOCK models was performed using molecular visualization tools to assess the quality of the binding interface. Particular attention was given to the presence of hydrogen bonds, hydrophobic contacts, and the proximity of the toxins to known functional or active sites on the channel. This combined approach of score-based ranking and structural validation was used then to identify the most plausible *vrdg*183-channel binding conformation (Fig. 5D and F). The results confirm that *vrdg*183 binds to the extracellular $L6_{IV}$ loop of the dome located in the outer pore region (Fig. 5D and F). The amino acid R18 of the C-terminal region of the toxin interacts with P1475, G1476 and K1477 of the channel. Moreover, G19 of the toxin interacts with K1477 (Table 5).

### 3.7. Molecular dynamics

The MD simulations were carried out by means of the HDOCK docking results, focused on these key aspects: whether the peptide remains stably positioned, how strong and consistent its interactions are with the surrounding residues, and whether it causes any structural changes that might affect ion flow.

The traces in black in Fig. 6A and B show the RMSD and Rg, respectively, of control simulations for the α1 channel subunit alone. RMSD kinetics demonstrate that the structure achieves conformational equilibrium near to 50 ns, remaining mostly stable afterwards. Similarly, Rg rapidly decreased over the first 50 ns in a process which then continued more gradually. Fig. 6C and D shows the final 3D conformation reached, subsequently used for comparison.

Interestingly, the analysis of the RMSD and Rg kinetics in the presence of the toxins reveals distinct dynamic behaviors for $Ca_v1.2$ when comparing to its unbound state. The channel bound to calciseptine (blue) displays relatively stable RMSD values throughout the simulation (Fig. 6A). In contrast, the *vrdg*183-channel complex (green) shows a gradual and sustained increase in RMSD, which reaches values about 30 % higher than for the unbound channel or the channel bound to calciseptine.

The Rg profiles of the calciseptine-channel complex (blue) and the *vrdg*183-channel complex (green) behave different from the unbound channel (black) as illustrated in Fig. 6B. The calciseptine-channel complex stabilizes about 1 Å below the profile of the native channel, early (8–10 ns from simulation start) departing from the control profile. When bound to *vrdg*183, there is a rapid decrease within the first 30 ns of the Rg simulation, generating a distinctive valley not present in the natural dynamics of the unbound channel. Although the *vrdg*183-channel profile almost superimposes to the control profile at the very end of the simulation, the kinetics are clearly different during the first 50 ns.

Structural snapshots from the final simulation frames show calciseptine positioned at the extracellular vestibule (Fig. 6E and F), but not directly occluding the pore. *vrdg*183 also binds at a peripheral site, away from the central ion-conducting pathway (Fig. 6G and H), reproducing the pose presented in the docking results.

Finally, the binding energies were −468.8 and −9.5 kJ/mol for calciseptine and *vrdg*183, respectively, suggesting a spontaneous process in both cases.

## 4. Discussion

Our main findings were: i) the venom gland of *P. verdolaga* has very low MW, disulfide-bridged peptides with effect on mammalian VGIC, ii)

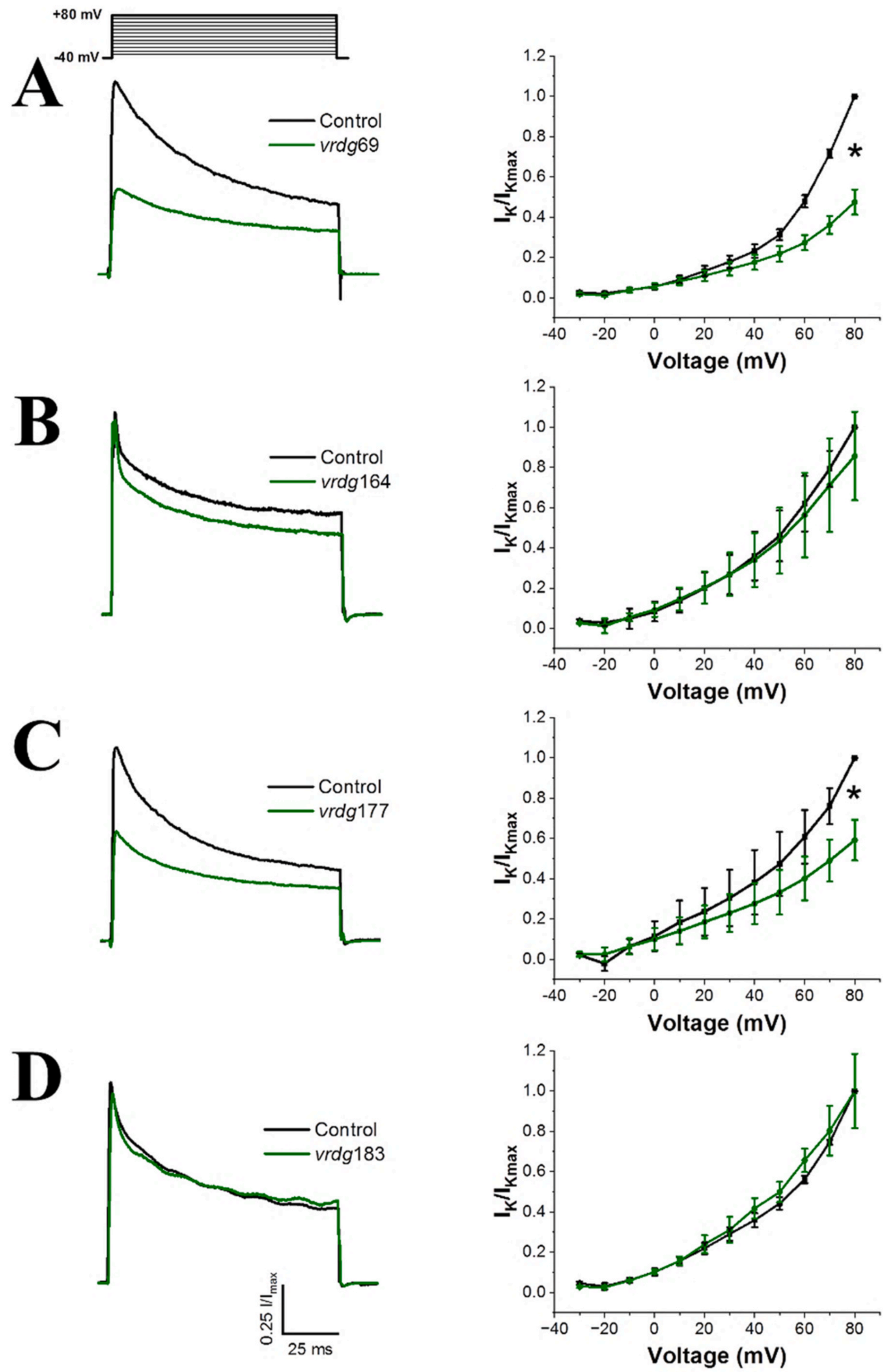


**Fig. 3. Selected normalized mean traces showing the effect of the *P. verdolaga* peptides on $I_K$.** Mean traces were generated by pooling all control (black) or experimental (*vrdg* peptides, green) records in one trace (left column), to summarize the effect of *vrdg*69 (**A**), *vrdg*164 (**B**), *vrdg*177 (**C**) and *vrdg*183 (**D**) on $I_K$ at +80 mV. The scale bar applies to all panels in the left column. The right column shows the corresponding current to voltage plots of the same toxins illustrated on the left. *vrdg*66 and *vrdg*172 were not shown because they look like *vrdg*183 and *vrdg*177, respectively. The upper insert represents the voltage step protocol used for stimulation. *P < 0.05, paired Student's *t*-test for current at +80 mV. $I_K$: $K^+$ current. (For interpretation of the references to color in this figure legend, the reader is referred to the Web version of this article.)

*vrdg*183 inhibits $I_{CaL}$ but not $I_{K,}$ iii) *vrdg*183 binds to the $L6_{IV}$ loop of the human $Ca_V1.2$, away from the channel pore, vi) *vrdg*69, *vrdg*164, *vrdg*172 and *vrdg*177 are unspecific inhibitors of VGIC.

### 4.1. New American spider toxins with very low MW

Spider VGIC-interacting toxins are underrepresented in the catalog of American toxins (Rojas-Palomino et al., 2024). The study of *P. verdolaga* (Theraphosidae) (Cifuentes et al., 2016) represents a valuable opportunity to identify novel toxins with potential to generate

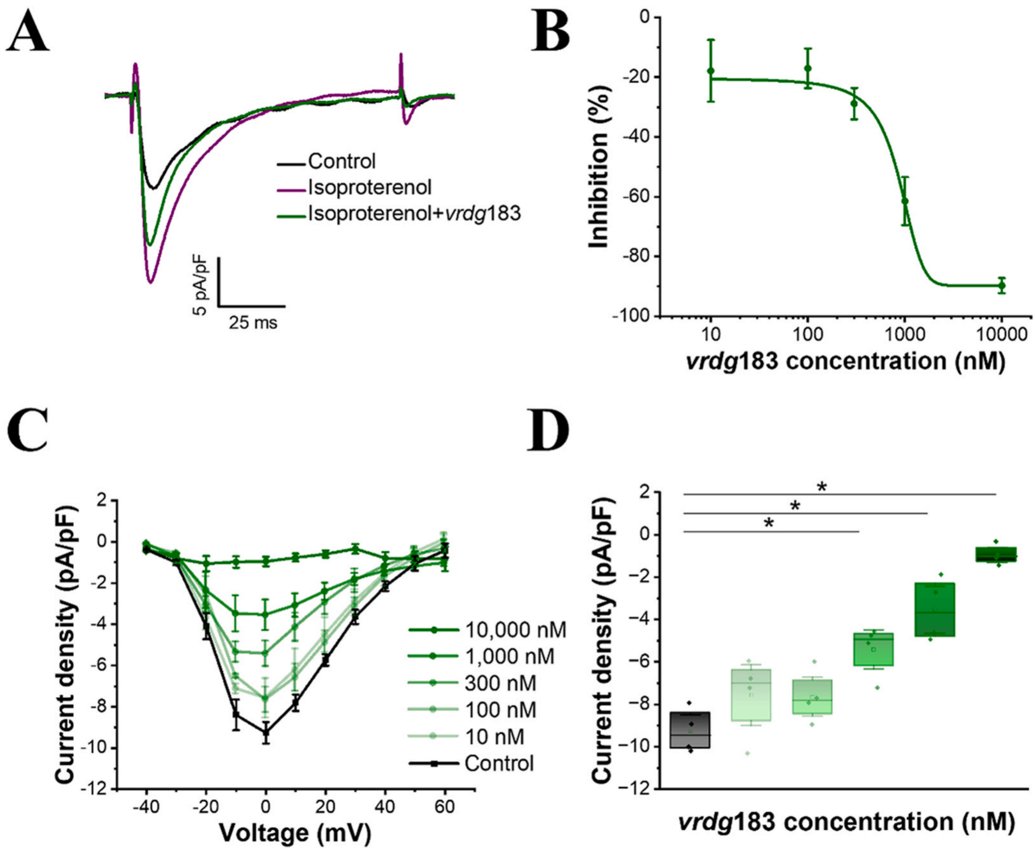


**Fig. 4. Characterization of the effect of *vrdg*183 on $I_{CaL}$. A.** Representative traces of the effect of *vrdg*183 (green) on $I_{CaL}$ prepotentiated by 100 μM isoproterenol. Isoproterenol increased the current density from −6.49 ± 1.21 to −14.30 ± 1.77 pA/pF. The subsequent application of 1 μM *vrdg*183 diminished the current amplitude to −10.50 ± 1.52 pA/pF ($P < 0.05$, one-way ANOVA). **B.** An $IC_{50}$ of 858.28 nM for the blockade of cardiac $I_{CaL}$ by *vrdg*183 was estimated through a sigmoidal fit (adjusted $R^2 = 0.99$) of the maximal currents obtained at increasing concentrations of the toxin at 0 mV. **C.** $I_{CaL}$ current to voltage plot obtained at the same increasing concentrations of *vrdg*183 used in B. No shift in the voltage at which the maximum current is reached was observed in the treatment conditions compared to the control and no obvious change in the reversal potential of the channel was observed, either. **D.** Box plots of the current density of $I_{CaL}$ at different concentrations of *vrdg*183 at 0 mV (*$P < 0.05$, one-way ANOVA followed by Tukey's post-hoc test). n = 4 for the experiments shown in all panels. $IC_{50}$: inhibitory concentration 50. $I_{CaL}$: L-type $Ca^{2+}$ current. (For interpretation of the references to color in this figure legend, the reader is referred to the Web version of this article.)

biological knowledge with pharmacological applications.

American spider toxins known to modulate VGCC and VGKC include ω-Grammotoxin-SIA from *Grammostola spatulate* (Theraphosidae), which potently inhibits $I_{CaP}$ ($IC_{50}$ ~50 nM) and $I_{CaN}$ ($IC_{50}$ ~500 nM) (McDonough et al., 1997), and Tx3-2 from *Phoneutria nigriventer* (Ctenidae), which blocks $I_{CaL}$ ($IC_{50}$ ~280 nM) (Kalapothakis et al., 1998). Ap2, Ap3 and Ap5 toxins from the Brazilian tarantula *Acanthoscurria paulensis* (Theraphosidae) block $Ca_v2.1$ ($I_{CaP/Q}$) with low potency ($IC_{50}$ over 1000 nM) (Tibery et al., 2021). Toxins within the class of ω-agatoxins, from *Agelenopsis aperta* (Agelenidae), influence $I_{CaL}$ and $I_{CaP/Q}$ (Adams, 2004). GiTx1 from *Grammostola iheringi* (Theraphosidae) blocks $I_K$ with low potency (Montandon et al., 2020) and PaTx1 and PaTx2 from *Phrixotrichus auratus* (Theraphosidae) are known to block cardiac $I_K$ (Diochot et al., 1999). The MW of these toxins ranges from ~3.5 to 6.0 kDa, in contrast to the smaller (~1.1 and 2.3 kDa) new toxins from *P. verdolaga*.

The global panorama is similar. According to ArachnoServer (August-2025), of the 869 putative spider toxin sequences with oxidized masses between 1.1 and 6.0 kDa, only 27 (3.1 %) fall within 1.1 and 2.3 kDa. Of them, 15 come from *Phoneutria nigriventer*. These numbers underscore how uncommon the reports of very low MW toxins are. Notably, *Phoneutria* and *Pamphobeteus* seem to be the only *geni* of the Araneae order, but still different family, experimentally explored and demonstrated to have very low MW toxins with effects on VGIC, suggesting that these peptides might have evolved all over the complete Araneae order. In sum, it is likely that many spider families, already studied or yet unexplored, have very low MW VGIC toxins awaiting to be discovered.

### 4.2. *vrdg183 is a novel $I_{CaL}$ inhibitor through an allosteric mechanism*

Although *vrdg*183 shares partial sequence identity with gomesin 1-18 (Silva et al., 2000), it does not have a sizeable antibacterial effect. Indeed, *vrdg*183 has minimum bactericidal concentrations against *E. Coli* and *P. aeruginosa* between 50 and 100 μM and had no effects against *S. aureus* and *E. faecalis* at the concentrations used in this study (Salinas-Restrepo et al., 2024). Similarly, *vrdg*183 produced less than 5 % hemolysis when tested between 1 and 3 μM (not shown), in agreement with the profile of gomesin (Silva et al., 2000). Moreover, no apparent acute cytotoxic effects were observed on cardiomyocytes upon *vrdg*183 exposure, either: there was not an increase in leak current or a change in the Rt or Cm at the end of the experiments. *vrdg*183 has a net positive charge and a low hydrophobic moment, which are typical features of peptides with low capacity of interaction with or insertion in the membrane. Overall, it seems that the effect of *vrdg*183 on $I_{CaL}$ is not mediated by peptide-lipid interactions or disruption of the cell membrane, as seen with other toxins (Grau-Campistany et al., 2016; Rojas-Palomino et al., 2025).

Instead, a mechanism mediated by peptide-peptide interactions was proved *in silico*. The RMSD and Rg profiles suggest a flexible interaction between *vrdg*183 and $Ca_v1.2$, indicative of an allosteric modulation, which induces a compaction of the channel (Lobanov et al., 2008). The

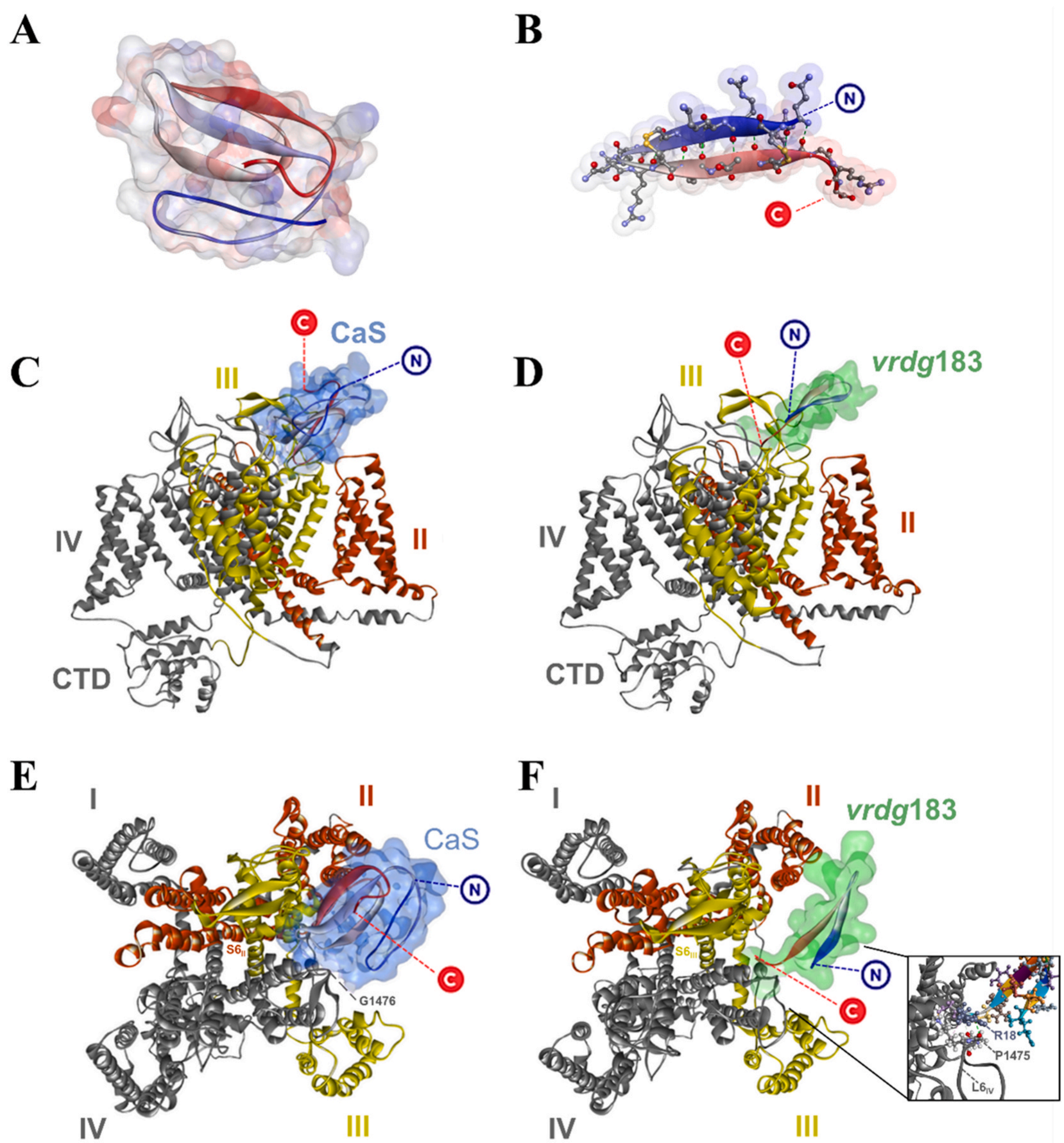


**Fig. 5. 3D structures and molecular docking. A.** Ribbon representation of the calciseptine 3D structure as generated with AlphaFold 3. **B.** *vrdg*183 3D structure obtained with AlphaFold 3. Disulfide bridges are highlighted in yellow and hydrogen bonds in green. The N- and C-terminals are also labeled. The per-atom confidence estimate was very high (>90) for the β-strands and the linker loop and was considered confident (>70) for the C-terminal free loop. **C.** Lateral view of the best binding pose for the calciseptine (CaS, blue)-channel (grey, yellow and red) complex. **D.** Lateral view of the best binding pose for the *vrdg*183-channel complex. **E.** Top view of the best binding pose for the CaS-channel complex. **F.** Top view of the best binding pose for the *vrdg*183-channel complex. Channel repeats I and IV appear in grey while repeats II and III appear in red and yellow respectively. $S6_{II}$, $S6_{III}$ and the kink of $L6_{IV}$ where G1476 is located are also identified. The insert in **F** zooms in a ball-and-stick representation of the binding among R18 (blue) and G19 (purple) of the C-terminal region of *vrdg*183 with the P1475, G1476 and K1477 (on the grey backbone) residues in the $L6_{IV}$ loop of the channel. The four toxin-channel interactions are indicated with thin colored (green, white, purple and orange) dotted lines. (For interpretation of the references to color in this figure legend, the reader is referred to the Web version of this article.)

**Table 3**
Pairs of amino acids involved in intramolecular hydrogen bonding in the structure of *vrdg*183

| Pair of aminoacids | Distance (Å) | Binding energy (kJ/mol) |
|---|---|---|
| **Q1-R16** | 2.24 | 18.03 |
| **Q1-R16** | 2.24 | 18.03 |
| **R3-Y14** | 1.72 | 25.00 |
| **R3-Y14** | 1.62 | 25.00 |
| **L5-L12** | 1.89 | 21.88 |
| **L5-L12** | 1.83 | 25.00 |
| **F7-R10** | 1.61 | 25.00 |
| **F7-R10** | 1.92 | 15.83 |

**Table 4**
Docking scores for calciseptine and *vrdg*183 obtained using ClusPro and HDOCK.

| Toxin | Calciseptine | | *vrdg*183 | |
|---|---|---|---|---|
| Docking method | ClusPro | HDOCK | ClusPro | HDOCK |
| **Score value** | −203.20 | −366.19 | −223.40 | −323.15 |
| **Confidence score** | 0.95 | 0.96 | 0.96 | 0.98 |

spatial separation between the toxin binding site and the permeation pathway supports an allosteric mechanism instead of a pore occlusion. *vrdg*183 binds to the $L6_{IV}$ loop, which is directly linked to $S6_{IV}$ on one side and to $P2_{IV}$ and the selectivity filter on the other side (Gao et al., 2023; Wu et al., 2016), therefore the conformational change induced by

**Table 5**
Pairs of amino acids involved in intermolecular interaction between *vrdg*183 and human $Ca_v1.2$.

| Pair of aminoacids (toxin-channel) | Distance (Å) | Type of interaction |
|---|---|---|
| **R18-P1475** | 2.24 | Hydrogen bond |
| **R18-G1476** | 2.85 | Hydrogen bond |
| **R18-K1477** | 4.30 | Alkyl bond |
| **G19-K1477** | 1.73 | Saline bond |

*vrdg*183 is expected to be allosterically transmitted from the dome to the pore of the channel. This mechanism further explains the fact that the *vrdg*183 effect on the channel was somewhat blunted in presence of isoproterenol. If the effect of the toxin were to directly block the pore, a profound effect of the toxin would have been observed even in presence of isoproterenol. Instead, the opening-favoring channel phosphorylation induced by isoproterenol seems to partially counteract the allosteric effect of the toxin. In agreement, the allosteric modulation is recognized as an important mechanism in $Ca^{2+}$ channel and $Ca^{2+}$ binding proteins pharmacology as well as in explaining the effect of toxins on different types of channels (Dilly et al., 2011; Eggan et al., 2024; Gao et al., 2023; Lai et al., 2015; Lyukmanova et al., 2023; Yang et al., 2014; Zhao et al., 2019).

Interestingly, both *vrdg*183 and calciseptine bind to $L6_{IV}$ by targeting G1476 and surrounding amino acids: P1475 and K1477 for *vrdg*183, and L1471 for calciseptine (Gao et al., 2023), suggesting that this channel region may be a hot-spot for the binding of $I_{CaL}$ regulating peptides. The larger size of calciseptine allows it to interact with other loops and helices of the channel, such as $L6_{III}$ or $P2_{IV}$, likely explaining why the $IC_{50}$ of calciseptine is lower (92 nM (Mesirca et al., 2024)) than the value of *vrdg*183. In summary, our results suggest that *vrdg*183 is a $Ca_v1.2$ channel inhibitor by acting as an allosteric pore modulator, trapping the channel in a non-conducting conformation, in a fashion similar to calciseptine.

*vrdg*183 blocked $I_{CaL}$ without affecting $I_K$, highlighting its potential as a pharmacological relevant lead compound. In fact, VGCC blockers, including peptide toxins, have shown antihypertensive and analgesic properties or have mitigated diabetic complications (Godfraind, 2017; López et al., 2019; Sousa et al., 2018; Wang et al., 2023). In fact, an effect on $Ca_v1.2$ leads to think on a potential modulation of excitation-contraction coupling and contractility, justifying a future characterization of the effect of *vrdg*183 on overall cardiac function. Given that not all $Ca_v$ isoforms share the binding sequence PGK, a high degree of specificity of *vrdg*183 is expected, something that must be tested in future experiments. Similarly, its effects on $K_v$ isoforms involved in cardiotoxicity (Grunnet, 2010; Skibsbye and Ravens, 2016), must be attested. Ultimately, following the rational nomenclature for spider toxins (King et al., 2008), we can rename *vrdg*183 as ω1.2-Phtx-Pv183a.

### *4.3. vrdg69, vrdg164, vrdg172, vrdg177 are unspecific VGIC inhibitors*

Since these peptides have similar physicochemical properties to *vrdg*183, a mechanism involving toxin-channels interactions is expected. However, *vrdg*164 prolonged the activation phase of $I_{CaL}$ and altered the I-V plot. Since an α-helical structure (not shown) can be predicted from its primary sequence, *vrdg*164 may also affect the lipid bilayer. Further studies are required to define the precise mechanisms of action of these toxins.

Given the plenty of $K_v$ isoforms that contribute to cardiac $I_K$, we cannot be certain about a specific isoform targeted by these peptides. However, we speculate that the main targets of these toxins are $K_v4.x$ isoforms (Guo et al., 2002). Further experiments in heterologous expression systems or artificial lipid bilayers can clarify this.

### *4.4. Strengths, limitations and final remarks*

The main strengths are: first, we employed patch-clamp, which is the gold standard technique to test the effect of isolated toxins on VGIC. All major biophysical properties of the cardiomyocytes and of cardiac $I_{CaL}$ and $I_K$ (*i.e.*, Cm, current kinetics, current density, *etc*) were consistent with previous descriptions (Benndorf et al., 1985; Gusev et al., 2009; Hussain and Orchard, 1997; Kumari et al., 2018; Mitcheson, 1998; Swift et al., 2012). Second, we used synthesized peptides, overcoming previous limitations for the study of spider toxins, such as the low efficiency of the purification procedures (Tibery et al., 2021). Lastly, the use of calciseptine as a control strengthened the *in silico* simulations and added original information to the field. The results were consistent with previous ones (Gao et al., 2023).

Some flaws in our work are: first, we did not systematically verify the order and complete formation of the cysteine bridges after purification. However, several lines of evidence confirm that they were well synthesized, oxidized and folded: the RP-HPLC chromatograms of the synthetized peptides, which can be seen elsewhere (Salinas-Restrepo et al., 2024), confirm the presence of two oxidation stages in the bridged peptides; the expected MS ions were actually experimentally observed; the RP-HPLC chromatogram of a control *vrdg*177 synthesized using Cys (acm) and tallium fluoroacetate to be in command of the oxidation process was similar to the chromatogram of the Cys(trt) peptide oxidized with DMSO used in the present assays; this *vrdg*177 was confirmed to have a β-folded structure by circular dichroism (not shown) and there was a difference between the effect of the control peptide *vrdg*66, selected from the transcriptomic analysis of the same spider but lacking disulfide bridges, and the other, bridged peptides. Second, there is a rundown of ∼5–10 % of the amplitude of the currents in the patch-clamp experiments, which explains in part the measurable effect of *vrdg*66. Moreover, this peptide induces a ∼12 % hemolysis at 1.5 μM (Salinas-Restrepo et al., 2024). Thus, the small effect of *vrdg*66 can be explained by adding up a small rundown and a slight permeabilization of the membrane. Third, we neither evaluated nor discussed the effect of the toxins on $I_{Na}$, limiting any conclusion about their specificity. Finally, the $IC_{50}$ and the molecular docking were not performed for all peptides. Certainly, each toxin deserves a dedicated work, something out of the scope of this paper.

## 5. Conclusion

A multidisciplinary approach allowed us to identify the first five toxins of the spider *P. verdolaga* which modulate VGIC. This report contributes to fill the gap in knowledge about the effect of very low MW animal toxins on VGIC. *vrdg*183 highlights as a moderately potent allosteric inhibitor of mammalian $I_{CaL}$ with no effect on $I_K$. Its promising specificity and low MW confer *vrdg*183 pharmacological interest.

## CRediT authorship contribution statement

**Alejandro Gómez-Restrepo:** Writing – review & editing, Visualization, Methodology, Formal analysis, Data curation. **Jessica Rojas-Palomino:** Writing – review & editing, Visualization, Methodology, Formal analysis, Data curation. **Cristian Salinas-Restrepo:** Writing – review & editing, Resources, Methodology. **César Segura:** Writing – review & editing, Resources. **Oscar A. Saurith-Coronell:** Visualization, Methodology. **Edgar A. Márquez-Brazón:** Writing – review & editing, Supervision, Methodology. **Marco A. Giraldo:** Supervision, Funding acquisition, Conceptualization. **Juan C. Calderón:** Writing – original draft, Supervision, Project administration, Funding acquisition, Formal analysis, Conceptualization.

## Ethics approval

All experimental procedures involving animals in this research were

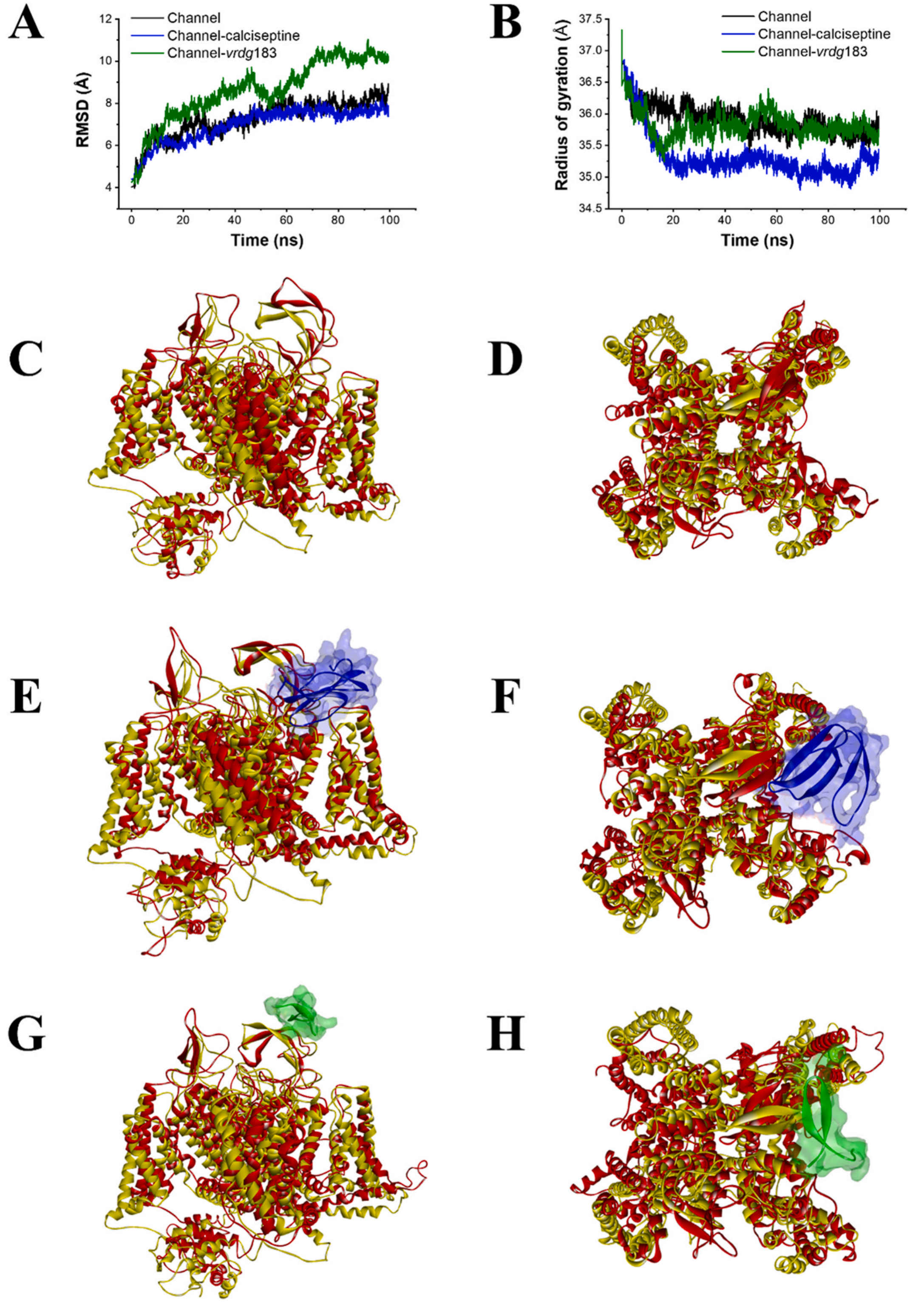


**Fig. 6. Molecular dynamic simulations of the interaction between calciseptine and *vrdg*183 with human $Ca_v1.2$.** **A.** Root-mean-square deviation (RMSD) profile of the intrinsic conformational behavior of $Ca_v1.2$ in absence of ligands (black) and in presence of calciseptine (blue) or *vrdg*183 (green). The notable increase in the values for *vrdg*183 confirms that this toxin induces more pronounced changes in the channel than calciseptine. **B.** Radius of gyration profile of the intrinsic conformational behavior of $Ca_v1.2$ in absence of ligands (black) and in presence of calciseptine (blue) or *vrdg*183 (green). The sustained decrease for calciseptine indicates a compaction of the channel, while the kinetics for *vrdg*183 suggests a larger peripheral rearrangement. **C, D.** Lateral and top view of the structural stability and compaction of $Ca_v1.2$ in the absence of inhibitors. The red-colored structure represents the final conformation of the channel after 100 ns of simulation, compared to the starting point (yellow). **E, F.** Lateral and top views of the initial (yellow) and final conformation (red) of the calciseptine-channel complex. **G, H.** Lateral and top views of the initial (yellow) and final conformation (red) of the *vrdg*183-channel complex. The final pose of the channel in the *vrdg*183-channel complex demonstrates large peripheral conformational changes in all repeats, while the changes were modest for calciseptine, agreeing with the results of the RMSD and radius of gyration. (For interpretation of the references to color in this figure legend, the reader is referred to the Web version of this article.)

approved by the institutional ethics committee for animal care of the University of Antioquia (minutes 129 of October 29$^{th}$ of 2019), Colombia. Animals were kept in polypropylene cages with access to food and water ad libitum, and light-dark cycles of 12:12 h. Only male Swiss Webster mice, weighing 20–26 g, were used. For euthanasia, animals were exposed to isoflurane (2 %) for 25–30 s before a rapid cervical dislocation was applied by a trained researcher.

## Consent for publication

Not applicable.

## Declaration of generative AI and AI-assisted technologies in the manuscript preparation process

The authors declare that they did not use generative AI at any stage of the preparation of this manuscript.

## Funding

This research was funded by the Colombian Ministry of Science and Technology (MinCiencias, Grant 111577757673, to JCC, MAG and CS), the Planning Office of the University of Antioquia, Colombia (grants E01792-B and ES03180101 to JCC and MAG), Colombia and the Instructor scholarship (2019–2020 to JR-P) from University of Antioquia, Colombia. Funders did not participate in selecting sources of evidence, analyses, manuscript writing or submission.

## Declaration of competing interest

The authors declare the following financial interests/personal relationships which may be considered as potential competing interests: Juan C. Calderon reports financial support was provided by Colombia Ministry of Science Technology and Innovation. If there are other authors, they declare that they have no known competing financial interests or personal relationships that could have appeared to influence the work reported in this paper.

## Acknowledgments

We thank Andrés Milán, Lorena Muñoz and Norman Balcázar (University of Antioquia), and Pura Bolaños (Venezuelan Institute of Scientific Research) for technical support.

## Data availability

The sequences of the peptides of the venom gland of *P. verdolaga* have already been made available in repositories by our groups (Salinas-Restrepo et al., 2024).

## References

Abramson, J., Adler, J., Dunger, J., Evans, R., Green, T., Pritzel, A., Ronneberger, O., Willmore, L., Ballard, A.J., Bambrick, J., Bodenstein, S.W., Evans, D.A., Hung, C.-C., O'Neill, M., Reiman, D., Tunyasuvunakool, K., Wu, Z., Žemgulytė, A., Arvaniti, E., Beattie, C., Bertolli, O., Bridgland, A., Cherepanov, A., Congreve, M., Cowen-Rivers, A.I., Cowie, A., Figurnov, M., Fuchs, F.B., Gladman, H., Jain, R., Khan, Y.A., Low, C.M.R., Perlin, K., Potapenko, A., Savy, P., Singh, S., Stecula, A., Thillaisundaram, A., Tong, C., Yakneen, S., Zhong, E.D., Zielinski, M., Žídek, A., Bapst, V., Kohli, P., Jaderberg, M., Hassabis, D., Jumper, J.M., 2024. Accurate structure prediction of biomolecular interactions with AlphaFold 3. Nature 630, 493–500. https://doi.org/10.1038/s41586-024-07487-w.

Adams, M.E., 2004. Agatoxins: ion channel specific toxins from the american funnel web spider, Agelenopsis aperta. Toxicon 43, 509–525. https://doi.org/10.1016/j.toxicon.2004.02.004.

Alexander, S.P., Mathie, A., Peters, J.A., Veale, E.L., Striessnig, J., Kelly, E., Armstrong, J. F., Faccenda, E., Harding, S.D., Pawson, A.J., Southan, C., Davies, J.A., Aldrich, R. W., Attali, B., Baggetta, A.M., Becirovic, E., Biel, M., Bill, R.M., Catterall, W.A., Conner, A.C., Davies, P., Delling, M., Virgilio, F. Di, Falzoni, S., Fenske, S., George, C., Goldstein, S.A.N., Grissmer, S., Ha, K., Hammelmann, V., Hanukoglu, I., Jarvis, M., Jensen, A.A., Kaczmarek, L.K., Kellenberger, S., Kennedy, C., King, B., Kitchen, P., Lynch, J.W., Perez-Reyes, E., Plant, L.D., Rash, L., Ren, D., Salman, M. M., Sivilotti, L.G., Smart, T.G., Snutch, T.P., Tian, J., Trimmer, J.S., Van den Eynde, C., Vriens, J., Wei, A.D., Winn, B.T., Wulff, H., Xu, H., Yue, L., Zhang, X., Zhu, M., 2021. The concise guide to pharmacology 2021/22: ion channels. Br. J. Pharmacol. 178, S157–S245. https://doi.org/10.1111/bph.15539.

Benndorf, K., Boldt, W., Nilius, B., 1985. Sodium current in single myocardial mouse cells. Pflugers Arch - Eur J Physiol 404, 190–196. https://doi.org/10.1007/BF00585418.

Bezanilla, F., 2008. How membrane proteins sense voltage. Nat. Rev. Mol. Cell Biol. 9, 323–332. https://doi.org/10.1038/nrm2376.

Bolaños, P., Calderón, J.C., 2022. Excitation-contraction coupling in mammalian skeletal muscle: blending old and last-decade research. Front. Physiol. 13, 989796. https://doi.org/10.3389/fphys.2022.989796.

Bolon, B., Heinz-Taheny, K., Yeung, K., Oguni, J., Erickson, T., Chai, P., Goldfine, C., 2023. Animal toxins. In: Heinz-taheny, K., Rudmann, D., Mahler, B. (Eds.), Haschek and Rousseaux's Handbook of Toxicologic Pathology. Academic Press, pp. 547–628.

Catterall, W.A., 1995. Structure and function of voltage-gated ion channels. Annu. Rev. Biochem. 64, 493–531. https://doi.org/10.1146/annurev.bi.64.070195.002425.

Cifuentes, Y., Estrada-Gomez, S., Vargas-Muñoz, L.J., Perafán, C., 2016. Description and molecular characterization of a new species of tarantula, Pamphobeteus verdolaga, from Colombia (Araneae: mygalomorphae: theraphosidae). Zool. 33, e20160113. https://doi.org/10.1590/s1984-4689zool-20160113.

Conforti, L., 2012. Patch-Clamp techniques. In: Sperelakis, N. (Ed.), Cell Physiology Source Book. Elsevier, pp. 369–381. https://doi.org/10.1016/B978-0-12-387738-3.00020-2.

Daly, N.L., Craik, D.J., 2011. Bioactive cystine knot proteins. Curr. Opin. Chem. Biol. 15, 362–368. https://doi.org/10.1016/j.cbpa.2011.02.008.

de Weille, J.R., Schweitz, H., Maes, P., Tartar, A., Lazdunski, M., 1991. Calciseptine, a peptide isolated from black mamba venom, is a specific blocker of the L-type calcium channel. Proc. Natl. Acad. Sci. U. S. A. 88, 2437–2440. https://doi.org/10.1073/pnas.88.6.2437.

Deplazes, E., 2017. Molecular simulations of disulfide-rich venom peptides with ion channels and membranes. Molecules 22, 362. https://doi.org/10.3390/molecules22030362.

Dilly, S., Lamy, C., Marrion, N.V., Liégeois, J., Seutin, V., 2011. Ion-Channel modulators: more diversity than previously thought. Chembiochem 12, 1808–1812. https://doi.org/10.1002/cbic.201100236.

Diochot, S., Drici, M.D., Moinier, D., Fink, M., Lazdunski, M., 1999. Effects of phrixotoxins on the Kv4 family of potassium channels and implications for the role of Ito1 in cardiac electrogenesis. Br. J. Pharmacol. 126, 251–263. https://doi.org/10.1038/sj.bjp.0702283.

Eggan, P., Gordon, S.E., Zagotta, W.N., 2024. Ligand-coupled conformational changes in a cyclic nucleotide-gated ion channel revealed by time-resolved transition metal ion FRET. eLife 13. https://doi.org/10.7554/eLife.99854.3.

Estrada-Gomez, S., Cardoso, F.C., Vargas-Muñoz, L., Quintana-Castillo, J., Arenas Gómez, C., Pineda, S., Saldarriaga-Cordoba, M., 2019. Venomic, transcriptomic, and bioactivity analyses of Pamphobeteus verdolaga venom reveal complex disulfide-rich peptides that modulate calcium channels. Toxins 11, 496. https://doi.org/10.3390/toxins11090496.

Estrada-Gomez, S., Vargas Muñoz, L.J., Quintana Castillo, J.C., 2013. Extraction and partial characterization of venom from the Colombian spider Pamphobeteus aff. nigricolor (Aranae:Theraphosidae). Toxicon 76, 301–309. https://doi.org/10.1016/j.toxicon.2013.10.014.

Gao, S., Yao, X., Chen, J., Huang, G., Fan, X., Xue, L., Li, Z., Wu, T., Zheng, Y., Huang, J., Jin, X., Wang, Y., Wang, Z., Yu, Y., Liu, L., Pan, X., Song, C., Yan, N., 2023. Structural basis for human Cav1.2 inhibition by multiple drugs and the neurotoxin calciseptine. Cell 186, 5363–5374.e16. https://doi.org/10.1016/j.cell.2023.10.007.

Godfraind, T., 2017. Discovery and development of calcium channel blockers. Front. Pharmacol. 8. https://doi.org/10.3389/fphar.2017.00286.

Grau-Campistany, A., Strandberg, E., Wadhwani, P., Rabanal, F., Ulrich, A.S., 2016. Extending the hydrophobic mismatch concept to amphiphilic membranolytic peptides. J. Phys. Chem. Lett. 7, 1116–1120. https://doi.org/10.1021/acs.jpclett.6b00136.

Grunnet, M., 2010. Repolarization of the cardiac action potential. Does an increase in repolarization capacity constitute a new anti-arrhythmic principle? Acta Physiol. 198, 1–48. https://doi.org/10.1111/j.1748-1716.2009.02072.x.

Guo, W., Li, H., Aimond, F., Johns, D.C., Rhodes, K.J., Trimmer, J.S., Nerbonne, J.M., 2002. Role of heteromultimers in the generation of myocardial transient Outward K + currents. Circ. Res. 90, 586–593. https://doi.org/10.1161/01.RES.0000012664.05949.E0.

Gusev, K., Ackermann, G., Heizmann, C., Niggli, E., 2009. Ca2+ signaling in mouse cardiomyocytes with ablated S100A1 protein. Gen. Physiol. Biophys. 28, 371–383. https://doi.org/10.4149/gpb_2009_04_371.

Guzmán, F., Gauna, A., Roman, T., Luna, O., Álvarez, C., Pareja-Barrueto, C., Mercado, L., Albericio, F., Cárdenas, C., 2021. Tea bags for fmoc solid-phase peptide synthesis: an example of circular economy. Molecules 26, 5035. https://doi.org/10.3390/molecules26165035.

Hamill, O.P., Marty, A., Neher, E., Sakmann, B., Sigworth, F.J., 1981. Improved patch-clamp techniques for high-resolution current recording from cells and cell-free membrane patches. Pflügers Archiv - Eur J Physiol 391, 85–100. https://doi.org/10.1007/BF00656997.

Hussain, M., Orchard, C.H., 1997. Sarcoplasmic reticulum Ca2+ content, L-type Ca2+ current and the Ca2+ transient in rat myocytes during β-adrenergic stimulation. J. Physiol. 505, 385–402. https://doi.org/10.1111/j.1469-7793.1997.385bb.x.

Jin, A.-H., Muttenthaler, M., Dutertre, S., Himaya, S.W.A., Kaas, Q., Craik, D.J., Lewis, R. J., Alewood, P.F., 2019. Conotoxins: chemistry and biology. Chem Rev 119, 11510–11549. https://doi.org/10.1021/acs.chemrev.9b00207.

Kalapothakis, E., Penaforte, C.L., Leão, R.M., Cruz, J.S., Prado, V.F., Cordeiro, M.N., Diniz, C.R., Romano-Silva, M.A., Prado, M.A.M., Gomez, M.V., Beirão, P.S.L., 1998. Cloning, cDNA sequence analysis and patch clamp studies of a toxin from the venom of the armed spider (Phoneutria nigriventer). Toxicon 36, 1971–1980. https://doi.org/10.1016/S0041-0101(98)00127-5.

King, G.F., Gentz, M.C., Escoubas, P., Nicholson, G.M., 2008. A rational nomenclature for naming peptide toxins from spiders and other venomous animals. Toxicon 52, 264–276. https://doi.org/10.1016/j.toxicon.2008.05.020.

King, G.F., Hardy, M.C., 2013. Spider-venom peptides: structure, pharmacology, and potential for control of insect pests. Annu. Rev. Entomol. 58, 475–496. https://doi.org/10.1146/annurev-ento-120811-153650.

Kodirov, S.A., 2023. Whole-cell patch-clamp recording and parameters. Biophys Rev 15, 257–288. https://doi.org/10.1007/s12551-023-01055-8.

Kumari, N., Gaur, H., Bhargava, A., 2018. Cardiac voltage gated calcium channels and their regulation by β-adrenergic signaling. Life Sci. 194, 139–149. https://doi.org/10.1016/j.lfs.2017.12.033.

Lacampagne, A., Duittoz, A., Bolaños, P., Peineau, N., Argibay, J., 1995. Effect of sulfhydryl oxidation on ionic and gating currents associated with L-type calcium channels in isolated guinea-pig ventricular myocytes. Cardiovasc. Res. 30, 799–806.

Lai, M., Brun, D., Edelstein, S.J., Le Novère, N., 2015. Modulation of Calmodulin lobes by different targets: an allosteric model with hemiconcerted conformational transitions. PLoS Comput. Biol. 11, e1004063. https://doi.org/10.1371/journal.pcbi.1004063.

Langenegger, N., Nentwig, W., Kuhn-Nentwig, L., 2019. Spider venom: components, modes of action, and novel strategies in transcriptomic and proteomic analyses. Toxins 11, 611. https://doi.org/10.3390/toxins11100611.

Lobanov, M.I., Bogatyreva, N.S., Galzitskaia, O.V., 2008. Radius of gyration is indicator of compactness of protein structure. Mol Biol (Mosk) 42, 701–706.

López, R., Bolaños, P., Guillén, A., Fernández, M.C., Ramos, M., Granados, S., Milán, A.F., Caputo, C., Alvarado-Castillo, C., Estrada, O., Calderón, J.C., 2019. Pomolic acid reduces contractility and modulates excitation-contraction coupling in rat cardiomyocytes. Eur. J. Pharmacol. 851, 88–98. https://doi.org/10.1016/J.EJPHAR.2019.02.016.

Lyukmanova, E.N., Zaigraev, M.M., Kulbatskii, D.S., Isaev, A.B., Kukushkin, I.D., Bychkov, M.L., Shulepko, M.A., Chugunov, A.O., Kirpichnikov, M.P., 2023. Molecular basis for Mambalgin-2 interaction with Heterotrimeric α-ENaC/ASIC1a/γ-ENaC channels in cancer cells. Toxins 15, 612. https://doi.org/10.3390/toxins15100612.

McDonough, S., Lampe, R., Keith, R., Bean, B., 1997. Voltage-Dependent inhibition of N- and P-Type calcium channels by the peptide toxin ω-Grammotoxin-SIA. Mol. Pharmacol. 52, 1095–1104. https://doi.org/10.1124/mol.52.6.1095.

Mesirca, P., Chemin, J., Barrère, C., Torre, E., Gallot, L., Monteil, A., Bidaud, I., Diochot, S., Lazdunski, M., Soong, T.W., Barrère-Lemaire, S., Mangoni, M.E., Nargeot, J., 2024. Selective blockade of Cav1.2 (α1C) versus Cav1.3 (α1D) L-type calcium channels by the black mamba toxin calciseptine. Nat. Commun. 15, 54. https://doi.org/10.1038/s41467-023-43502-w.

Mitcheson, J., 1998. Cultured adult cardiac myocytes future applications, culture methods, morphological and electrophysiological properties. Cardiovasc. Res. 39, 280–300. https://doi.org/10.1016/S0008-6363(98)00128-X.

Montandon, G.G., Cassoli, J.S., Peigneur, S., Verano-Braga, T., Santos, D.M. dos, Paiva, A. L.B., Moraes, É.R. de, Kushmerick, C., Borges, M.H., Richardson, M., Pimenta, A.M. de C., Kjeldsen, F., Diniz, M.R.V., Tytgat, J., Lima, M.E. de, 2020. GiTx1 (β/κ-theraphotoxin-Gi1a), a novel toxin from the venom of Brazilian tarantula Grammostola iheringi (Mygalomorphae, Theraphosidae): isolation, structural assessments and activity on voltage-gated ion channels. Biochimie 176, 138–149. https://doi.org/10.1016/j.biochi.2020.07.008.

Morin, T.J., Kobertz, W.R., 2008. A derivatized scorpion toxin reveals the functional output of heteromeric KCNQ1-KCNE K+ channel complexes. ACS Chem. Biol. 2, 469–473. https://doi.org/10.1021/cb700089s.

Ochoa, R., Brown, J.B., Fox, T., 2023. pyPept: a python library to generate atomistic 2D and 3D representations of peptides. J Cheminform 15, 79. https://doi.org/10.1186/s13321-023-00748-2.

Percie du Sert, N., Hurst, V., Ahluwalia, A., Alam, S., Avey, M.T., Baker, M., Browne, W. J., Clark, A., Cuthill, I.C., Dirnagl, U., Emerson, M., Garner, P., Holgate, S.T., Howells, D.W., Karp, N.A., Lazic, S.E., Lidster, K., MacCallum, C.J., Macleod, M., Pearl, E.J., Petersen, O.H., Rawle, F., Reynolds, P., Rooney, K., Sena, E.S., Silberberg, S.D., Steckler, T., Würbel, H., 2020. The ARRIVE guidelines 2.0: updated guidelines for reporting animal research. J. Physiol. 598, 3793–3801. https://doi.org/10.1113/JP280389.

Porter, K.A., Xia, B., Beglov, D., Bohnuud, T., Alam, N., Schueler-Furman, O., Kozakov, D., 2017. ClusPro PeptiDock: efficient global docking of peptide recognition motifs using FFT. Bioinformatics 33, 3299–3301. https://doi.org/10.1093/bioinformatics/btx216.

Quintana, E., Torres, Y., Alvarez, C., Rojas, A., Forero, M.E., Camacho, M., 2010. Changes in macrophage membrane properties during early Leishmania amazonensis infection differ from those observed during established infection and are partially explained by phagocytosis. Exp. Parasitol. 124, 258–264. https://doi.org/10.1016/j.exppara.2009.10.006.

Quintero-Hernández, V., Jiménez-Vargas, J.M., Gurrola, G.B., Valdivia, H.H., Possani, L. D., 2013. Scorpion venom components that affect ion-channels function. Toxicon 76, 328–342. https://doi.org/10.1016/j.toxicon.2013.07.012.

Rash, L.D., Hodgson, W.C., 2002. Pharmacology and biochemistry of spider venoms. Toxicon 40, 225–254. https://doi.org/10.1016/S0041-0101(01)00199-4.

Rojas-Palomino, J., Altuna-Alvarez, J., González-Magaña, A., Queralt-Martín, M., Albesa-Jové, D., Alcaraz, A., 2025. Electrophysiological dissection of the ion channel activity of the Pseudomonas aeruginosa ionophore protein toxin Tse5. Chem. Phys. Lipids 267, 105472. https://doi.org/10.1016/j.chemphyslip.2025.105472.

Rojas-Palomino, J., Gómez-Restrepo, A., Salinas-Restrepo, C., Segura, C., Giraldo, M.A., Calderón, J.C., 2024. Electrophysiological evaluation of the effect of peptide toxins on voltage-gated ion channels: a scoping review on theoretical and methodological aspects with focus on the Central and South American experience. J. Venom. Anim. Toxins Incl. Trop. Dis. 30, e20230048. https://doi.org/10.1590/1678-9199-jvatitd-2023-0048.

Salinas-Restrepo, C., Misas, E., Estrada-Gómez, S., Quintana-Castillo, J.C., Guzman, F., Calderón, J.C., Giraldo, M.A., Segura, C., 2022. Improving the annotation of the venom Gland transcriptome of Pamphobeteus verdolaga, prospecting novel bioactive peptides. Toxins 14, 408. https://doi.org/10.3390/toxins14060408.

Salinas-Restrepo, C., Naranjo-Duran, A.M., Quintana, J., Bueno, J., Guzman, F., Hoyos Palacio, L.M., Segura, C., 2024. Short antimicrobial peptide derived from the venom Gland transcriptome of Pamphobeteus verdolaga increases gentamicin susceptibility of multidrug-resistant Klebsiella pneumoniae. Antibiotics 13, 6. https://doi.org/10.3390/antibiotics13010006.

Sierra-Hernandez, O., Saurith-Coronell, O., Rodríguez-Macías, J., Márquez, E., Mora, J. R., Paz, J.L., Flores-Sumoza, M., Mendoza-Mendoza, A., Flores-Morales, V., Marrero-Ponce, Y., Barigye, S.J., Martinez-Rios, F., 2025. In silico identification of potential clovibactin-like antibiotics binding to unique cell Wall precursors in diverse gram-positive bacterial strains. Int. J. Mol. Sci. 26, 1724. https://doi.org/10.3390/ijms26041724.

Silva, P.I., Daffre, S., Bulet, P., 2000. Isolation and characterization of gomesin, an 18-Residue cysteine-rich defense peptide from the spider Acanthoscurria gomesiana hemocytes with sequence similarities to Horseshoe crab antimicrobial peptides of the Tachyplesin family. J. Biol. Chem. 275, 33464–33470. https://doi.org/10.1074/jbc.M001491200.

Skibsbye, L., Ravens, U., 2016. Mechanism of proarrhythmic effects of potassium channel blockers. Card Electrophysiol Clin 8, 395–410. https://doi.org/10.1016/j.ccep.2016.02.004.

Sousa, S.R., McArthur, J.R., Brust, A., Bhola, R.F., Rosengren, K.J., Ragnarsson, L., Dutertre, S., Alewood, P.F., Christie, M.J., Adams, D.J., Vetter, I., Lewis, R.J., 2018. Novel analgesic ω-conotoxins from the vermivorous cone snail Conus moncuri provide new insights into the evolution of conopeptides. Sci. Rep. 8, 13397. https://doi.org/10.1038/s41598-018-31245-4.

Swift, F., Franzini-Armstrong, C., Øyehaug, L., Enger, U.H., Andersson, K.B., Christensen, G., Sejersted, O.M., Louch, W.E., 2012. Extreme sarcoplasmic reticulum volume loss and compensatory T-tubule remodeling after Serca2 knockout. Proc. Natl. Acad. Sci. USA. 109, 3997–4001. https://doi.org/10.1073/pnas.1120172109.

Tibery, D.V., de Souza, A.C.B., Mourão, C.B.F., do Nascimento, J.M., Schwartz, E.F., 2021. Purification and characterization of peptides Ap2, Ap3 and Ap5 (ω-toxins) from the venom of the Brazilian tarantula Acanthoscurria paulensis. Peptides (N.Y.) 145, 170622. https://doi.org/10.1016/j.peptides.2021.170622.

Wang, Y.C., Wang, L., Shao, Y.Q., Weng, S.J., Yang, X.L., Zhong, Y.M., 2023. Exendin-4 promotes retinal ganglion cell survival and function by inhibiting calcium channels in experimental diabetes. iScience 26, 107680. https://doi.org/10.1016/j.isci.2023.107680.

Wu, J., Yan, Z., Li, Z., Qian, X., Lu, S., Dong, M., Zhou, Q., Yan, N., 2016. Structure of the voltage-gated calcium channel Cav1.1 at 3.6 Å resolution. Nature 537, 191–196. https://doi.org/10.1038/nature19321.

Xia, Z., He, D., Wu, Y., Kwok, H.F., Cao, Z., 2023. Scorpion venom peptides: molecular diversity, structural characteristics, and therapeutic use from channelopathies to viral infections and cancers. Pharmacol. Res. 197, 106978. https://doi.org/10.1016/j.phrs.2023.106978.

Yan, Y., Tao, H., He, J., Huang, S.-Y., 2020. The HDOCK server for integrated protein–protein docking. Nat. Protoc. 15, 1829–1852. https://doi.org/10.1038/s41596-020-0312-x.

Yang, P.S., Johny, M. Ben, Yue, D.T., 2014. Allostery in Ca2+ channel modulation by calcium-binding proteins. Nat. Chem. Biol. 10, 231–238. https://doi.org/10.1038/nchembio.1436.

Zhang, J., Diamond, S., Arvedson, T., Sasu, B.J., Miranda, L.P., 2010. Oxidative folding of hepcidin at acidic pH. Biopolymers 94, 257–264. https://doi.org/10.1002/bip.21383.

Zhao, L., Lai, L., Zhang, Z., 2019. How calcium ion binding induces the conformational transition of the calmodulin N-terminal domain—an atomic level characterization. Phys. Chem. Chem. Phys. 21, 19795–19804. https://doi.org/10.1039/C9CP03917A.